Journal of Saudi Chemical Society (2018) **22**, 826–837

King Saud University

Journal of Saudi Chemical Society

www.ksu.edu.sa
www.sciencedirect.com

ORIGINAL ARTICLE

Influence of ZnO doping on structural, optical and pH-stimulus characteristics of silica-titania nanocomposite matrix

Shumaila Islam [a], Hazri Bakhtiar [a,*], Noriah Bidin [a], Ali Aqeel Salim [a], Saira Riaz [b], Khaldoon N. Abbas [a,c], Lau Pik Suan [a], Shahzad Naseem [b]

[a] *Laser Centre, Ibnu Sina Institute for Scientific and Industrial Research, Universiti Teknologi Malaysia, Skudai, Johor 81310 Malaysia*
[b] *Centre of Excellence in Solid State Physics, University of the Punjab, Lahore, Pakistan*
[c] *Al-Mustansiriya University, Faculty of Science, Physics Department, Baghdad 00964, Iraq*

Received 4 October 2017; revised 30 December 2017; accepted 21 January 2018
Available online 31 January 2018

KEYWORDS

Silica-titania nanocomposite;
ZnO doping;
Structural and optical properties;
Fiber optic sensing

Abstract In-situ sol-gel procedure is used to synthesize the silica-titania nanocomposite (SiO_2-TiO_2) as host matrix which is doped with ZnO and heated at 300 °C for 1 h for homogeneous and stable matrix surface. The mixture of organic dyes i.e. cresol red, bromophenol blue, phenol red and phenolphthalein is encapsulated within ZnO:SiO_2-TiO_2 nanocomposite for the evaluation of sensing activity at dynamic pH range 1–12. Microscopic findings showed that the synthesized nanocomposites have homogeneous crack-free porous coating with low roughness value of 9.7–7.6 nm. XRD analysis shows the formation of new phase $ZnSiO_3$ after ZnO doping and heat treatment along with anatase phase of titania and silica. TEM analysis confirmed the spherical nanoparticles. The heterogeneous bonding of synthesized Zn:SiO_2-TiO_2 composites is investigated by FTIR. Surface analysis confirmed that prepared nanocomposites have high surface area, large pore diameters and mesoporous nature, which is desirable for good sensing behavior. Optical studies show that low refractive index (1.33–1.39) transparent nanocomposites (92–62% transparency in the visible range) are promising for sensing applications. TGA analysis shows that SiO_2-TiO_2 nanocomposites after ZnO doping and heat treatment are thermally stable. The fast response 0.15 s of the ZnO:SiO_2-TiO_2 nanocomposite coated fiber optic sensor is optimized at pH 12. The observed sensitivity is of 15 counts/pH with repeatability of 93% at 440 nm.
© 2018 King Saud University. Production and hosting by Elsevier B.V. This is an open access article under the CC BY-NC-ND license (http://creativecommons.org/licenses/by-nc-nd/4.0/).

* Corresponding author.
E-mail addresses: shumaila@utm.my (S. Islam), hazri@utm.my (H. Bakhtiar), noriah@utm.my (N. Bidin), saira.cssp@pu.edu.pk (S. Riaz), laupiksuan-pd@utm.my (L.P. Suan), Director.cssp@pu.edu.pk (S. Naseem).
Peer review under responsibility of King Saud University.

ELSEVIER Production and hosting by Elsevier

https://doi.org/10.1016/j.jscs.2018.01.005
1319-6103 © 2018 King Saud University. Production and hosting by Elsevier B.V.
This is an open access article under the CC BY-NC-ND license (http://creativecommons.org/licenses/by-nc-nd/4.0/).

1. Introduction

Recently, inorganic-organic composites have received considerable attention due to their exciting properties including chemical and thermal stability of composite matrices with a homogeneous pore distribution, particle size/shapes, transparency, mechanical strength, with unique application orientations in chemical, biomedicine, optics and sensing fields [1–4]. Moreover, metal-organic nanocomposites' synthesis by several methods including vapor deposition, imprinted, hydrothermal synthesis, microwave synthesis or thermal decomposition method has been reported so far [5–12]. However, these techniques lower the sensitivity for the analyte and prolong the response time of the sensor. Sol-gel method is well known for the synthesis of sensing materials with good chemical and thermal stability without cracking/leaching, longer operational lifetime, good controlling of the physical and chemical parameters such as time dependent morphology, crystallinity and controlled porosity [13–15]. Generally, the contribution of nanocomposite matrix for sensing activities is strictly dependent on crack-free morphology with low roughness, high surface area, low refractive index, nanoparticle size distribution and accessibility of the active sites leads to improve the characteristics and properties of sensing material, such as selectivity, sensibility, accuracy, response time and useful life, which broaden the scope of the sensor's applications [13].

Silica-titania nanocomposite has good mechanical strength, high surface coverage, high thermal stability and transparency, good dispersibility in solvents, porosity and tunable refractive index [2]. Therefore, porous silica-titania nanocomposite as oxidation catalyst and for sensing applications has special interest in academic and industrial field [16,17]. For sensing applications, a mesoporous high surface area structure is desirable in combination with low roughness, chemical stability and refractive index. Moreover, ZnO is one of the most promising materials due to its photosensitivity, chemical stability, fast electron transport capability and better light absorption compared to TiO_2 [1]. Therefore, ZnO doped silica-titania nanocomposite (Zn: SiO_2-TiO_2) was selected because of their unique properties such as low optical losses, high area mesoporous structure and difference in refractive index, which is required for energy and environment materials, including chemical sensors, photocatalysts, dye sensitization and perovskite solar cells [18–20]. The doping of surface active agent mixing in the composite can reduce the surface tension of the sol and enforced the polymerizing gel formation [2]. Consequently, highly porous and low refractive index nanocomposites can be synthesized with better sensing performances.

Furthermore, cresol red, bromophenol blue, phenol red and phenolphthalein were chosen due to their absorption and emission effective behavior toward the ionic strength. These dyes are found to be best to stimulate the behavior of the sensor, such as its suitability, permeability of the analyte and reagent immobilization. Encapsulation of indicator dyes within the nanocomposite matrix allows continued sensing without contamination, gives good adhesion with direct coating on optic fibers and easy for concentration measurements with species detections by diffusion, so it is possible to coupling optics and natural process make detectors and photonic devices. In the present report, it is found that structural and optical properties of prepared nanocomposite significantly depend on doping. To the authors' best knowledge, the synthesis of ZnO-doped SiO_2-TiO_2 nanocomposite matrix by sol-gel route for pH sensor applications with broad dynamic range has been rarely reported. This work could provide a novel avenue to the synthesis of multi-nanocomposite with colonial structure at low temperatures with distinguished properties, offering a new material platform for sensing and other applications.

2. Experimental

2.1. Synthesis of the sols

Tetraethylorthosilicate (TEOS) [98% Aldrich], titanium tetraisopropoxide (TTIP) [97% Aldrich], Zinc acetate (Zn $(CH_3CO_2)_2 2H_2O$) [99.8% Aldrich], were used as precursors of silica, titania and Zinc oxide, respectively. Isopropanol (Grade GC, 99.7%) and Anhydrous ethanol [99% Aldrich] were used as solvents and complexing agents, whereas, nitric acid [65% Merck] was used as a gelation acid catalyst (for enhanced hydrolysis and condensation process), determines the type of gel microstructure. The surfactant CTAB was used as the modifying agent. For sensing purpose, 2 ml of 0.5 M concentration of cresol red, bromophenol blue, phenol red and phenolphthalein indicator dyes mixture was encapsulated in silica-titania (1:1 ratio) sol mixture.

For silica sol, 40 ml of TEOS (Tetraethylorthosilicate) was mixed in the mixture of 25 ml of deionized water and 20 ml of ethanol (EtOH) for hydrolysis. 1 ml of HNO_3 (as catalyst) was added in the stirred solution and heated at 70 °C for 1 h. The molar ratios were TEOS: H_2O C_2H_5OH::HNO_3∼0.5:3.0:2.0:0.1. The sol was aged for 1 day. The pH of the resultant sol was acidic. For TiO_2 nanoparticles, 10 ml of TTIP was added into 20 ml of isopropanol (C_3H_7OH) for the partial hydrolysis. Afterward, 20 ml of propanol was added into the 10 ml of distilled water in the presence of HNO_3. Molar ratios for TiO_2 sol was TTIP:C_3H_7OH:H_2O:HNO_3 = 1.0:4.0:1.0:0.5. The solution was stirred at 100 °C for 1 h. For SiO_2- TiO_2 nanocomposite sol, SiO_2 sol and TiO_2 sol was mixed with 1:1 ratio and stirred it at 80 °C for 1 h, pH of nanocomposite was adjusted at pH 1. The mixed sol was then allowed to age for 24 h.

ZnO nanoparticles were synthesized by dissolving 0.2 g of zinc acetate [$Zn(CH_3CO_2)_2 2H_2O$] into a mixture of 30 mL of isopropyl alcohol, 10 ml of de-ionized water and 1 ml of nitric acid. Mixed solution was stirred at 70 °C for 60 min and then left it at room temperature for aging. Molar ratio for zinc sol was $Zn(CH_3CO_2)_2 2H_2O$:C_3H_7OH:H_2O:HNO_3 = 1.0:4.0:1.0:0.5., the pH was adjusted to <1. For doping, 10 ml of prepared ZnO sol was added into 50 ml of SiO_2-TiO_2 nanocomposite sol. 1 ml of 0.5 M concentration of CTAB solution was added under continuous stirring in the solution. For sensing purpose, 1 ml of 0.5 M concentration of CTAB solution and 2 ml of 0.5 M concentration of indicators solution (cresol red, bromophenol blue, phenol red, and phenolphthalein) were added drop wise into ZnO doped mixed silica-titania sol followed by stirring and heated at 80 °C for 1 h, the mixture was left at room temperature for several days for its appropriate aging cycles. All outlines of prepared sols are shown in Fig. 1(a).

The pH sensor device was prepared by dripping the sol (coating) on 5 cm decladed region of 35 cm long PCS (Plastic

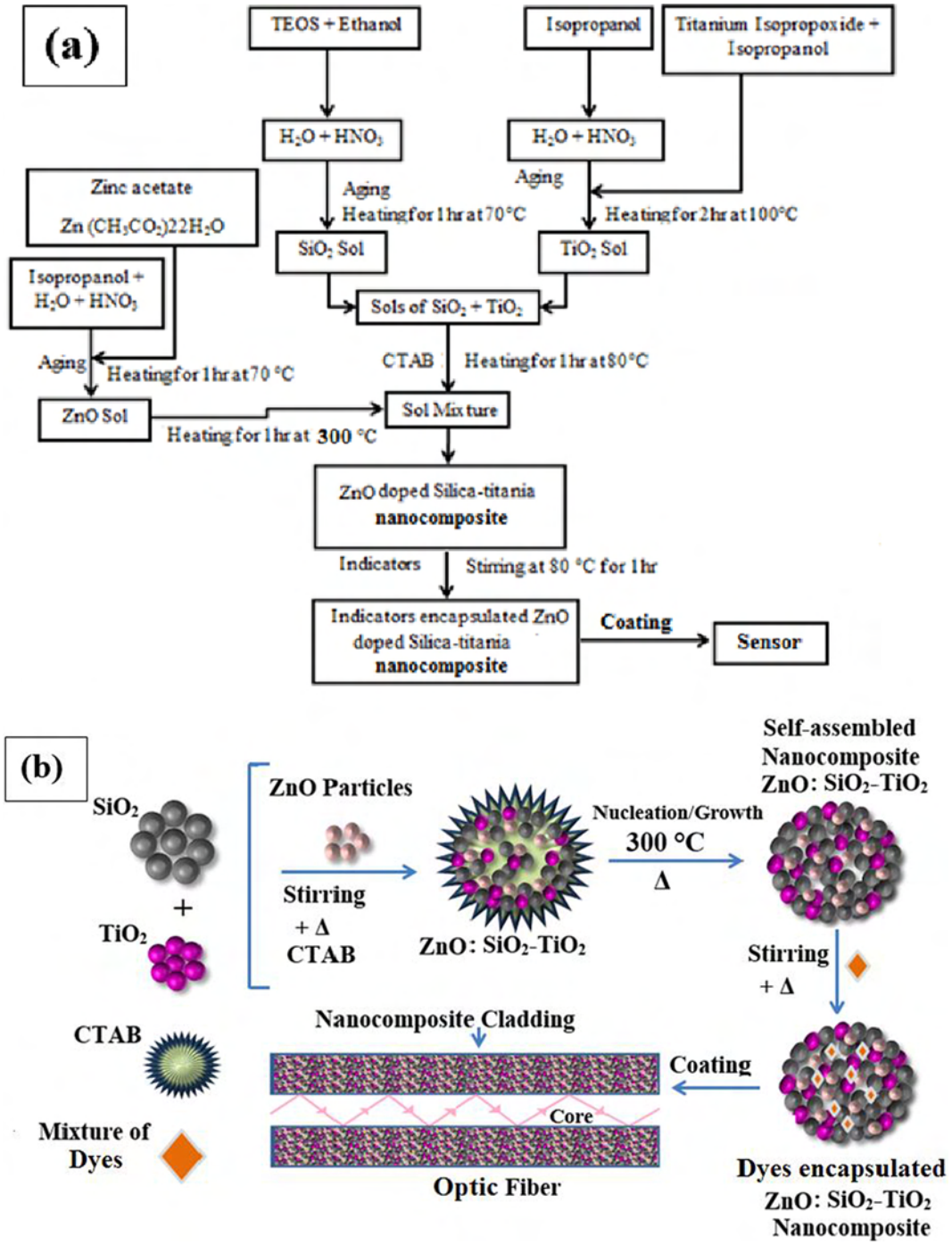

Fig. 1 ZnO doped SiO_2-TiO_2 nanocomposite (a) synthesis process layout (b) schematic representation.

Clad Silica) optical fiber, 1012 μm core diameter with NA = 0.37 ± 0.02 and 1.45 core refractive index. Both ends of the fiber were polished for the constancy in the coupling behavior of the launched light into the fiber. Prior to coating, 5 cm decladed region of fiber and glass substrates (for thin film characterizations) were cleaned by HNO_3 for 5 min and then rinsed several times with de-ionized water. After acid etching, in ultrasonic bath, the glass substrates were cleaned for 10 min by acetone and 20 min by isopropanol in order to remove organic contaminants. After cleaning, the sol was spin coated on glass substrates for 30 s at a rate of 4000 rpm using Delta 6RC Suss Microtec Spin Coater, at room temperature. For fiber coating, the prepared sol was manually dripped on fiber. The coated substrates were dried at room temperature for several days. Before sensing measurements, the coated fiber was washed with water in order to remove the excess and unbound dye species.

ZnO doped SiO_2-TiO_2 as host matrix for dyes encapsulation as new pH sensitive material is schemed in Fig. 1(b) using the sol–gel method. The surfactant CTAB was used as structure modifying agent for smooth/homogeneous surface of prepared nanocomposite and also can be used to protect the dyes

from fading [21]. Due to chemical doping, dye species probably uniformly distributed throughout the nanocomposite and not just residing on the surface as illustrated in schematic representation [Fig. 1(b)]. It has the advantage that the dye species are also reacted reversibly when the coated sensing region is in contact with an aqueous solution or with acidic or basic species as well.

3. Characterizations

Prepared nanocomposites' shapes and sizes were observed using Field emission scanning electron microscope (FE-SEM) SU8020. The average roughness (Ra), roots mean square roughness (RMS) and topography of un-doped and ZnO-doped SiO_2-TiO_2 nanocomposite thin films were analyzed by atomic force microscope equipment SPI 3800N, tapping-mode under ambient conditions. The scanned $1 \times 1\ \mu m^2$ area was analyzed by NanoNavi software version 5.01C. EDX spectra (Oxford Silicon Drift Detecto SDD) were used to know the percentage of elements present in the sample. Biological transmission electron microscopy (BIO-TEM) was employed for morphology and particle size observations. The prepared nanocomposites were mixed within ethanol and sonicated for 20 min, and then were collected onto carbon coated copper grids. The micrographs were observed on a HITACHI (HT7700) machine operating at 80 kV with Dock version 3.2 image analyses (software package). Structurally, the samples were characterized by PANalytical X'PERT PRO MRD PW 3040/60. Cu Kα (λ = 1.5405 Å) was used as target material. The incorporation of ZnO doping into SiO_2-TiO_2 matrix was verified by FTIR spectrophotometer (PerkinElmer Series L160000A), within the range of 4000 cm^{-1}–450 cm^{-1}. Brunauer, Emmett and Teller (BET) multipoint method and N_2 adsorption-desorption isotherms were employed for the surface areas of prepared samples and Barret, Joyner and Halenda (BJH) method was used to calculate the pore size distribution. The degradation process and the thermal stability of prepared nanocomposites were investigated by Thermogravimetric analysis (TGA) and differential thermal analysis (DTA) using thermogravimetric analyzer Mettler Toledo TGA851. The samples were heated from ~30 °C to ~1000 °C at the rate of 10 °C/min in the nitrogen atmosphere. Ultraviolet–visible transmission spectra of coated thin films were measured by spectrophotometer (Shimadzu UV-3101PC) in the range of 350–700 nm with ±3 nm accuracy. For data collection, bare glass substrate was used as reference. For sensing analysis, light source i.e., white light emitting diode was used and USB2000 miniature fiber optical spectrum analyzer was used to detect the wavelength characteristics. The dynamic range and progressive response of the sensor in various pH environments was investigated using a photospectrometer.

4. Results and discussions

FE-SEM micrographs of SiO_2-TiO_2, ZnO: SiO_2-TiO_2 and after heat treatment of ZnO: SiO_2-TiO_2 nanocomposites are shown in Fig. 2(a–c). Homogeneous surface morphology of SiO_2-TiO_2 spherical shaped nanoparticles without voids was revealed [Fig. 2(a)]. Moreover, Fig. 2(d) is the magnified area of Fig. 2(a), tiny deposits over the surface may be present due to the formation of their respective oxides. Whereas, ZnO:SiO_2-TiO_2 shows spherical shaped composite's cluster formation [Fig. 2(b)], aggregation of composite's cluster with pores is observed in Fig. 2(e) which is the zoomed area of Fig. 2(b), may be due to the adsorbed water molecules (on the composite's surface). After heat treatment of ZnO:SiO_2-TiO_2 at 300 °C for 1 h, the surface aspects are converted into interconnected colonies [Fig. 2(c)], where smaller spherical particle incorporation can be clearly seen within the larger particles/clusters, whereas, Fig. 2(f) is the magnified area of Fig. 2 (c), shows porosity within the colonies with small spherical nanoparticles. The changes in morphology are probably due to the nucleation growth that can result in a large surface-to-volume ratio. Additionally, in all images, the prepared materials exhibit well-ordered porous structures; mostly pores serve as active centers within the composites, valuable for improving the sensing properties as documented in literature [22].

In order to identify the elemental composition of SiO_2-TiO_2, ZnO: SiO_2-TiO_2 composite and after heat treatment of ZnO:SiO_2-TiO_2, Energy Dispersive X-ray (EDX) analysis was used. Fig. 2(g, h, i) shows the EDX spectra for all three nanocomposites. EDX analysis reveals the variations of Si, Ti, O along with Zn in doped samples, confirms the good incorporation between Zn, Si and Ti lattices. The values of elements are summarized in Table 1. Pt signals belong to the top coating on synthesized thin films which was applied for FE-SEM analysis. Moreover, no other impurities were found on the surface of the composite suggesting that the synthesized nanocomposites were relatively pure.

AFM 3-D images of SiO_2-TiO_2 nanocomposite, ZnO:SiO_2-TiO_2 nanocomposite and ZnO:SiO_2-TiO_2 nanocomposite after 1 h heating at 300 °C, are illustrated in Fig. 3(a–c). Surface topography, average surface roughness (Ra) and root mean square roughness parameters (RMS) were evaluated for the scanned surface area of $1 \times 1\ \mu m^2$. SiO_2-TiO_2 nanocomposite [Fig. 3(a)] exhibits porous clusters morphology with an average surface roughness of 9.7 nm. However, the average surface roughness slightly decreases to a value of 7.6 nm after ZnO doping and influence the smoothness of SiO_2-TiO_2 nanocomposite [Fig. 3(b)]. It can be observed that after doping, nanoparticles are more uniform and well distributed. No cracked surface or voids were observed in the vicinity of crystals. Moreover, after heat treatment, it continuously decreased up to 5.7 nm [Fig. 3(c)], indicating that nanocomposite enclosures the Zn molecules, resulting in prominent nanoparticle appearance which is also documented in the literature [23].

TEM images of SiO_2-TiO_2 nanocomposite, ZnO doped SiO_2-TiO_2 nanocomposite and ZnO doped SiO_2-TiO_2 nanocomposite after 1 h heating at 300 °C, are shown in Fig. 4(a–c). It can be clearly seen that all three samples have spherical shape for the individual particles. A low degree of coalescence/coagulation is also observed. Coalescence refers to the fusion of two or more particles to form a single spherical particle [24]. Particle size distribution curves as shown in Fig. 4 (d, e, f) exhibited particle size ~3.89 nm ± 0.12 nm, 4.35 nm ± 0.22 nm and 5.43 nm ± 0.25 nm for SiO_2-TiO_2 nanocomposite, ZnO: SiO_2-TiO_2 nanocomposite and after heat treatment of ZnO: SiO_2-TiO_2 nanocomposite, respectively. SiO_2-TiO_2 nanocomposite shows the small particle size, according to literature it could be due to the solvent (ethanol) as short chain alcohols leads the production of small particle size [25]. However, after doping the particle size is increased

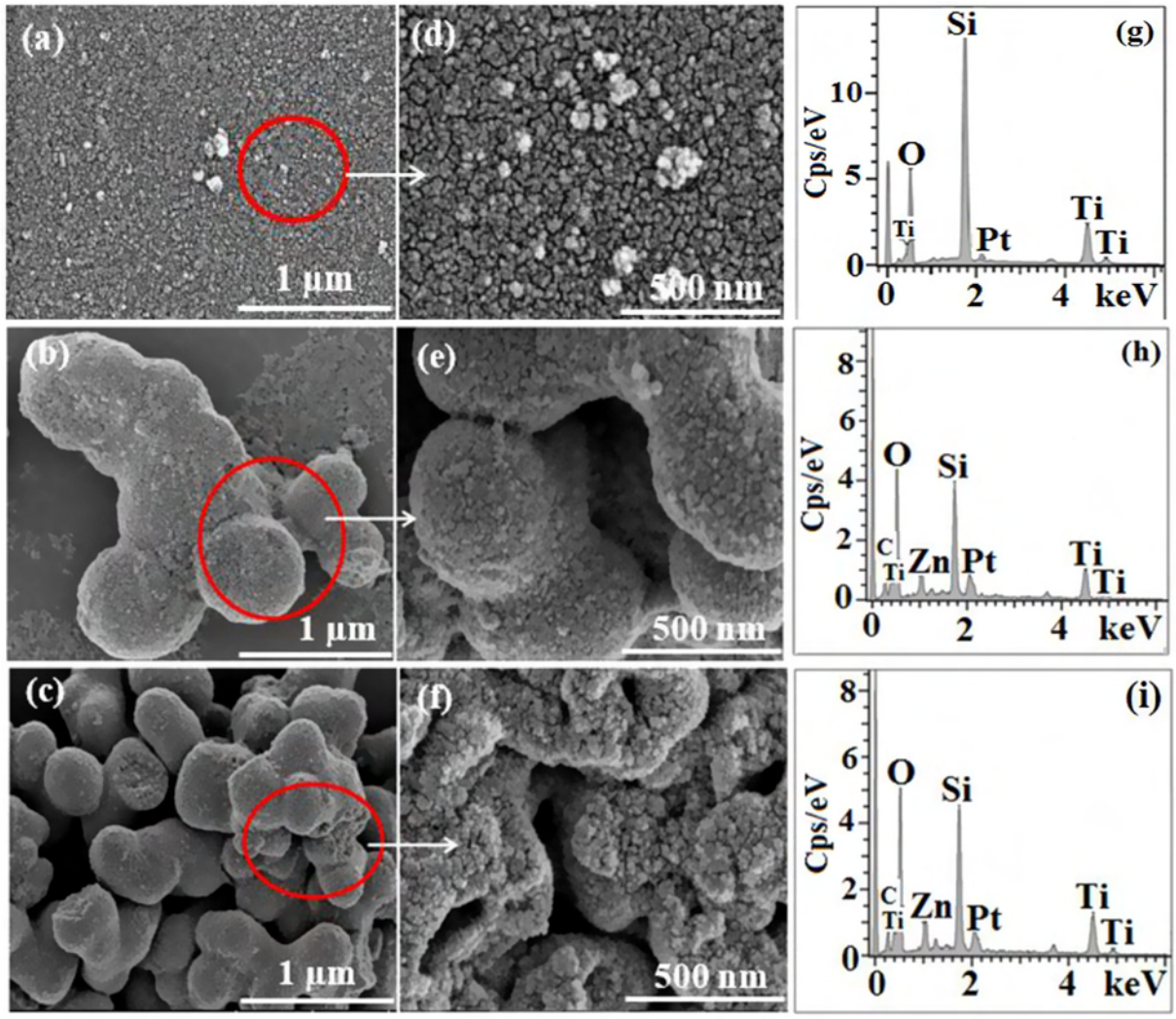

Fig. 2 FE-SEM micrographs of (a) SiO_2-TiO_2 (b) ZnO: SiO_2-TiO_2 (c) after heat treatment of ZnO: SiO_2-TiO_2 composite, (d, e, f) are the magnified areas of (a, b, c), whereas, (g, h, i) corresponding to the EDX spectra of (a, b, c), respectively.

Table 1 EDX analysis of SiO_2-TiO_2, ZnO: SiO_2-TiO_2 and after heat treatment of ZnO: SiO_2-TiO_2 nanocomposite.

Elements Wt.%	O	Si	Ti	C	Zn
SiO_2-TiO_2	16.3	37.9	39.1	6.7	–
ZnO: SiO_2-TiO_2	22.3	34.4	26.2	11.7	5.4
ZnO: SiO_2-TiO_2 after heat treatment	21.2	27.1	36.5	8.9	6.1

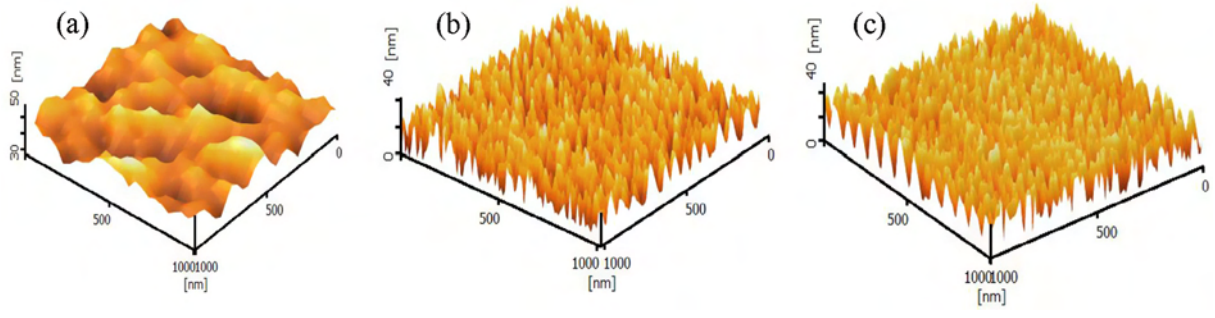

Fig. 3 AFM images of (a) SiO_2-TiO_2 nanocomposite (b) ZnO: SiO_2-TiO_2 nanocomposite (c) ZnO: SiO_2-TiO_2 nanocomposite after 1 h heating at 300 °C.

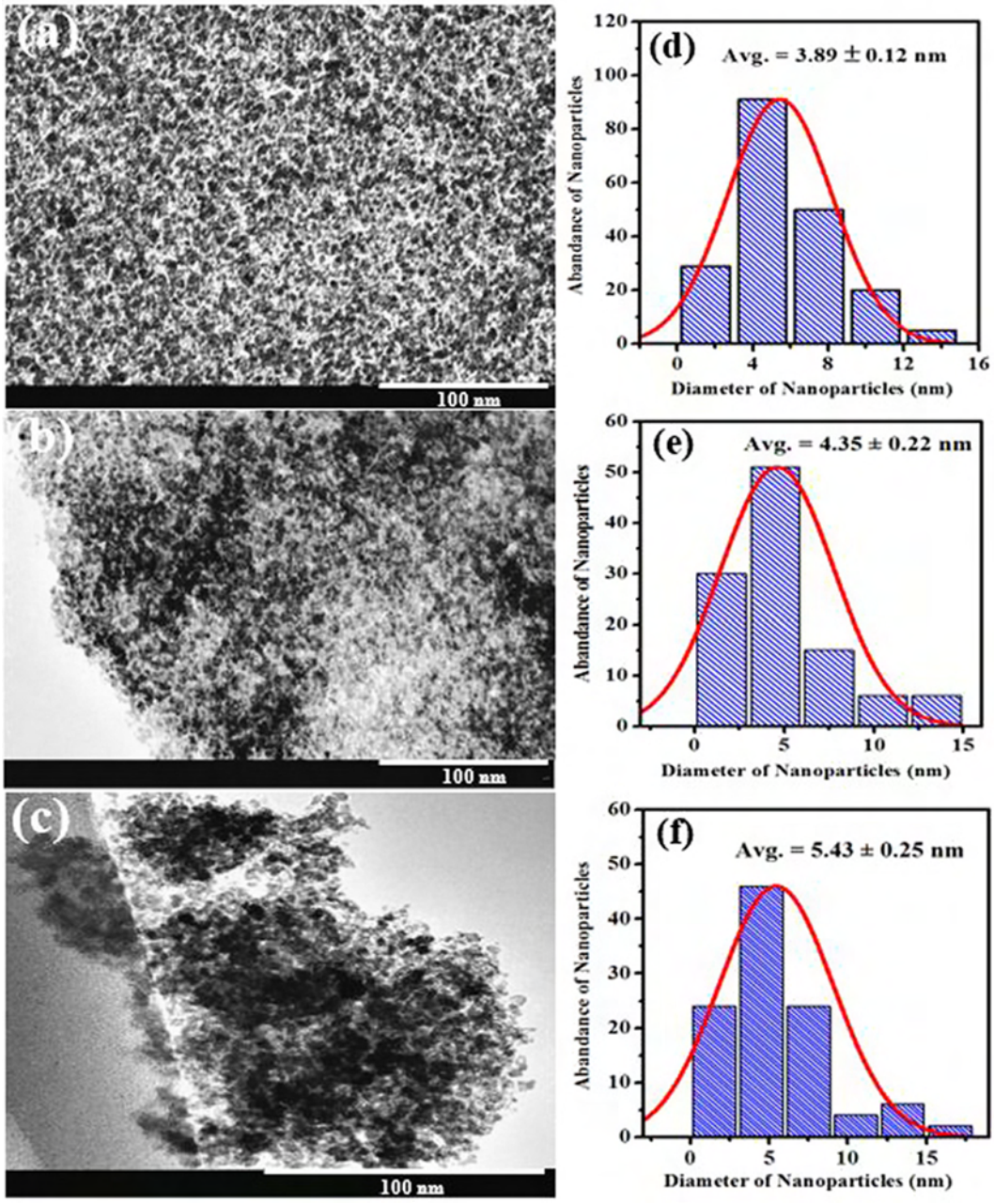

Fig. 4 TEM micrographs of (a) SiO_2-TiO_2 nanocomposite (b) ZnO: SiO_2 TiO_2 nanocomposite (c) ZnO: SiO_2-TiO_2 nanocomposite after 1 h heating at 300 °C, whereas, (d, e, f) corresponding to the histograms of (a, b, c) while, curve is the Gaussian fit.

[Fig. 4(e)], suggesting that ZnO doping facilitate the proper reaction between SiO_2 and the TiO_2 species, leading to the growth of nanoparticles. Fig. 4(f) illustrates the histogram of ZnO: SiO_2-TiO_2 nanocomposite after heat treatment, where average particles size increased around 5.43 nm ± 0.25 nm, agglomeration caused the enhancement in particle size. Basically, nucleation process leads to the particle coalescence from dissolved species; this results in formation of large particles. Moreover, Thirumavalava et al. [26] explained that a large particle size after heat treatment results from the finite extent and particular morphology of the coherently diffracting domains within the grains. However, the structure morphology after heat treatment is well distributed and spherical in shape.

Fig. 5-I(a–c) shows the XRD graphs of SiO_2-TiO_2 nanocomposite, ZnO doped SiO_2-TiO_2 nanocomposite and ZnO doped SiO_2-TiO_2 nanocomposite after 1 h heating at 300 °C, respectively. All three nanocomposites show a high intense peak with (1 0 1) plane and low intense peak with (2 1 1) plane of SiO_2 (JCPDS 15-26). Several prominent peaks of TiO_2 in all three samples are also observed [Fig. 5-I(a–c)]. Planes (1 0 1), (0 0 4), (2 0 0), (2 1 1) and (2 0 4) corresponding to anatase phase of TiO_2 (JCPDS 21-1276). After ZnO doping in SiO_2-TiO_2 nanocomposite, few peaks of $ZnSiO_3$ phase are appeared with planes of (0 1 5), (0 2 4) and (1 1 6) (JCPDS 034-0575) [Fig. 5-II(b)], suggesting the SiO_2-TiO_2 nanocomposite network incorporation with the ZnO particles. After

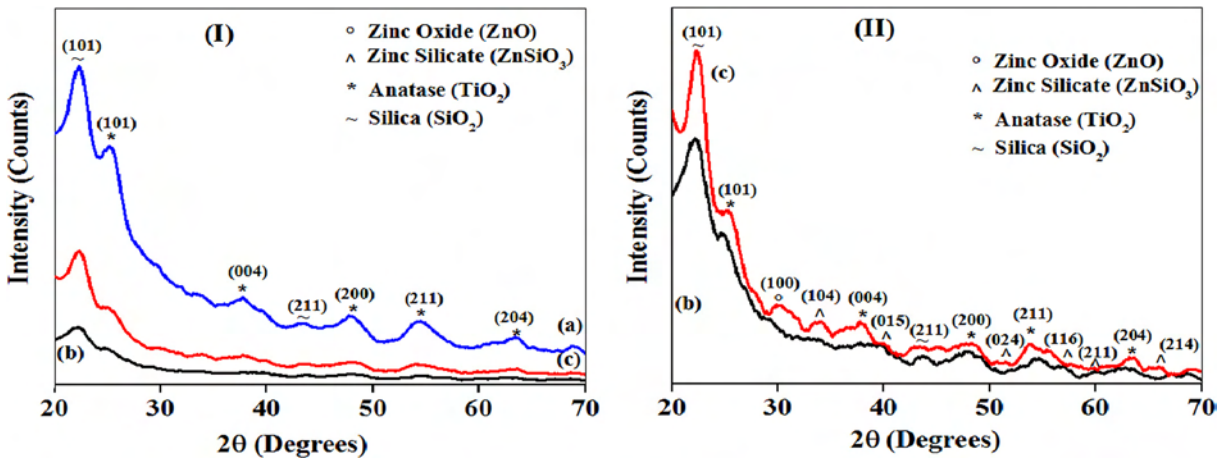

Fig. 5 (I) XRD graphs of (a) SiO_2-TiO_2 nanocomposite (b) ZnO: SiO_2-TiO_2nanocomposite (c) ZnO: SiO_2-TiO_2 nanocomposite after 1 h heating at 300 °C, whereas, (II) corresponding to the zoomed image of b and c.

heat treatment, many peaks of $ZnSiO_3$ phase corresponding to (1 0 4), (2 1 1) and (2 1 4) are also observed [Fig. 5-II(c)]. A prominent peak of ZnO with (1 0 0) plane (JCPDS 01-075-0576) is also observed. So, it can be inferred that annealing plays a vital role in phase variation with strength and crystalline growth of nanocomposites. The crystallite size of SiO_2-TiO_2 nanocomposite, ZnO doped SiO_2-TiO_2 nanocomposite and after 1 h heating at 300 °C was calculated using Debye-Scherer formula

$$D = k\lambda/\beta\cos\theta$$

where, λ is the wavelength, k is the shape factor taken as 0.9, θ is the diffraction angle and β is the full width at half maximum. The (1 0 1) plane positioned ~22.2° in all three samples was chosen to calculate the crystalline size. Crystallite size ~ 10.80 nm of SiO_2-TiO_2 nanocomposite was calculated, while, ~ crystallite size ~ 12.44 nm was observed after ZnO doping in SiO_2-TiO_2 nanocomposite. However, the crystallite size increased up-to ~23.51 nm after heat treatment. These observations indicate that the crystallinity of the SiO_2-TiO_2 nanocomposite increased after ZnO doping and heat treatment which is due to the particle nucleation and growth process. In literature, it is stated that according to LaMer theory, the particle formation depends on nucleation process which is responsible for particle coalescence from dissolved species; and results in larger particles from nanoparticle growth [27,28]. Therefore, a larger crystallite size was observed after heat treatment.

FTIR spectra of SiO_2-TiO_2 nanocomposite, ZnO: SiO_2-TiO_2 nanocomposite and Zn: SiO_2-TiO_2 nanocomposite after 1 h heat treatment at 300 °C is shown in Fig. 6(a–c), respectively. Mostly, metal oxides exhibited absorption bands in fingerprint region (i.e. below 1000 cm^{-1}), which arise from interatomic vibrations [29]. In this context, a small band appearance at 466 cm^{-1} in SiO_2-TiO_2 nanocomposite is associated with the symmetric Si-O-Si siloxane groups' vibrations as also reported in the literature [30]. A little intense band at 764 cm^{-1} is due to the stretching mode of Ti–O–Ti in SiO_2-TiO_2 nanocomposite. The bands around at 965 cm^{-1} in SiO_2-TiO_2 nanocomposite are associated with the stretching mode of Ti–O–Si linkage, as documented in the literature [31]. Since, free ZnO is not detected in the composite system which suggested that it has a better connectivity between the SiO_2-TiO_2 building units. A sharp band ~1095 cm^{-1} in SiO_2-TiO_2 nanocomposite can be associated with the transverse optical vibration mode corresponding to the asymmetric stretching of the inter tetrahedral oxygen atoms in the Si–O–Si linkage, had in fact shifted toward the lower wavenumber ~ 1072 cm^{-1} after ZnO doping and around 1040 cm^{-1} after heat treatment, has been associated with the incorporation of Zn molecules with the SiO_2, TiO_2 species. This confirms the successful bonding between SiO_2, TiO_2 and ZnO species. Moreover, the band located around 1386 cm^{-1} in SiO_2-TiO_2 nanocomposite, 1381 cm^{-1} after ZnO doping and around 1395 cm^{-1} after heat treatment is probably due to the existing of C–O–C bands. In SiO_2-TiO_2 nanocomposite, the peak observed at 1639 cm^{-1}, shifted toward the lower wavenumber around 1633 cm^{-1} and 1626 cm^{-1} with high intensity after ZnO doping and heat treatment after 1 h at 300 °C. These variations in the peak wave number are characteristic of a C═O group, which expose the interactions of carbonyl functional group with doping species. Moreover, the bands around 2856 cm^{-1} and 2915 cm^{-1} in the SiO_2-TiO_2 nanocomposite which is shifted to 2851 cm^{-1} and 2921 cm^{-1} after heat treatment is ascribed to the C–H

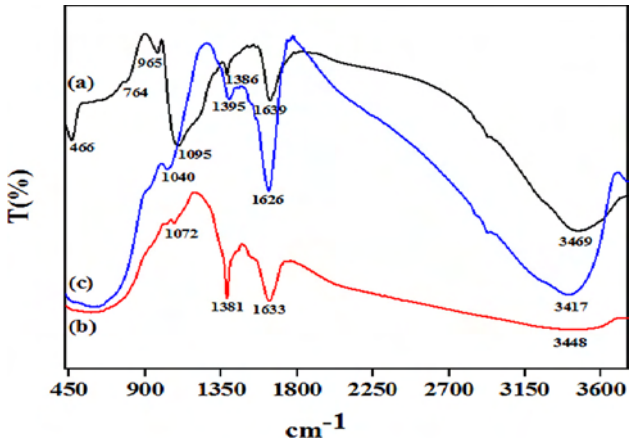

Fig. 6 FTIR spectra of (a) SiO_2-TiO_2 nanocomposite (b) ZnO doped SiO_2-TiO_2 nanocomposite (c) ZnO doped SiO_2-TiO_2 nanocomposite after 1 h heating at 300 °C.

stretching vibrations, resulted from the $-CH_2$ and $-CH_3$ in the organic solvents. The broad band around 3417 cm^{-1}–3469 cm^{-1} in all three samples is attributed to the major stretching vibrations of adsorbed hydroxyl groups from water molecules or probably due to ethanol residues. However, the peak broadness around 3448 cm^{-1} in ZnO: SiO_2-TiO_2 nanocomposite is diminished, which indicates the decrease of water and stability of composite.

BET surface analysis shows that SiO_2-TiO_2 nanocomposite has a high surface area ~ 441 m^2/g, large pore volume ~ 0.69 cm^3/g, BET pore diameter ~ 62.97 Å and BJH pore diameter ~ 58.53 Å. High surface areas and large pore volumes in order to host the large objects and anchoring molecular functions, as well as for fast mass diffusion and transfer, are desirable for sensing [32]. However, after ZnO-doping, the surface area is reduced to 283 m^2/g, pore volume ~ 0.23 cm^3/g, BET pore diameter ~ 33.20 Å and BJH pore diameter ~ 32.87 Å, probably due to the filling of SiO_2-TiO_2 nanocomposite pores by the Zn-species and formed a new phase i.e. $ZnSiO_3$ as confirmed by XRD analysis. While, after heat treatment, the surface area

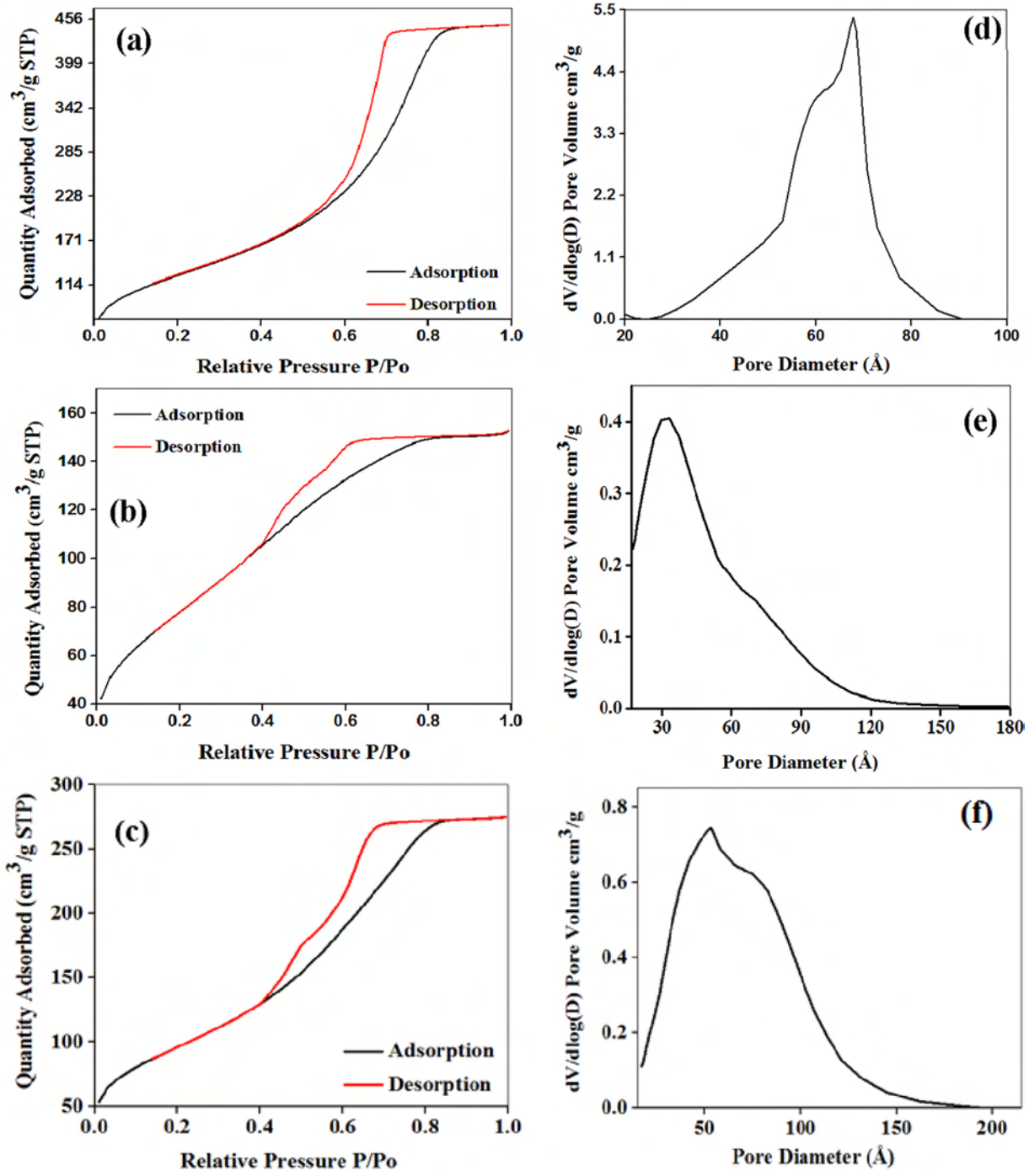

Fig. 7 N_2 adsorption-desorption isotherm of (a) SiO_2-TiO_2 nanocomposite (b) ZnO: SiO_2-TiO_2 nanocomposite (c) ZnO: SiO_2-TiO_2 nanocomposite after 1 h heating at 300 °C, (I, II, III) corresponding to the BJH pore size distribution of (a, b, c), respectively.

is increased up-to ~345 m^2/g, and pore volume ~ 0.40 cm^3/g, BET average pore diameter ~ 49.3 Å, BJH average pore diameter ~ 45.86 Å is also found to be increased. The variations in these parameters are due to the nucleation and growth of particles (strength of the $ZnSiO_3$ phase).

Fig. 7(a–c) are the representative of N_2 adsorption-desorption isotherms for SiO_2-TiO_2 nanocomposite, ZnO: SiO_2-TiO_2 nanocomposite and ZnO: SiO_2-TiO_2 nanocomposite after 1 h heating at 300 °C, respectively. Typically, strength of fluid–wall and fluid–fluid interaction and pore space is responsible for the determination of isotherm's shape. Synthesized SiO_2-TiO_2 [Fig. 7(a)] is found to be Type IV with H_2 hysteresis loop in the range of 0.45–1.0P/Po (P is the partial pressure of the adsorbate and the Po is adsorbent saturated vapor pressure), whereas, ZnO: SiO_2-TiO_2 nanocomposite shows H_2 hysteresis loop in the range of 0.4–1.0P/Po [Fig. 7 (b)], owing to occurrence of capillary condensation within the pores followed by saturation as the pores become filled with liquid (complete pore filling) in mesopores of both samples. Generally, shape of an isotherm reflects the way in which the water binds the system. Weaker water molecule interactions generate a greater water activity, thus, the material shows more instability [33]. After heat treatment, the ZnO: SiO_2-TiO_2 nanocomposite also shows Type IV with H_2 hysteresis loop in the range of 0.4–1.0 [Fig. 7(c)]. The obtained uniform porosity ensures that the enhanced reaction rates are probably due to the high level of interaction between Zn, Si and Ti active sites. Moreover, the sharp peak of SiO_2-TiO_2 nanocomposite BJH pore size [Fig. 7(d)] suggest the presence of uniform accessible narrowly distributed pores in size and representative of mesoporous materials as documented in the literature [34], whereas, after ZnO doping and heat treatment [Fig. 7(e, f)] the nanocomposites show pronounced pore size peak in the mesoporous region 20 Å–500 Å according to IUPAC (International Union of Pure and Applied Chemistry).

The UV–visible transmittance spectra of SiO_2-TiO_2, ZnO: SiO_2-TiO_2 nanocomposite and ZnO:SiO_2-TiO_2 nanocomposite after 1 h heating at 300 °C are illustrated in Fig. 8-I(a–c). It clearly indicates that the optical absorption band ~ 545 nm in SiO_2-TiO_2 nanocomposite is shifted toward a higher wavelength ~ 631 nm after Zn doping and heat treatment, probably due to particles' cluster formation. Transmission ~ 93% is observed in SiO_2-TiO_2 nanocomposite which is reduced to ~ 62% at wavelength of 550 nm after ZnO doping but it increased again up to ~ 78% after heat treatment. Furthermore, Fresnel equation was used to calculate the refractive indices of prepared samples. The dispersion of the refractive indices is shown in Fig. 8-II(a–c). The calculated refractive index of SiO_2-TiO_2 nanocomposite is 1.33 at 550 nm, which is increased up to 1.39 at 550 nm after ZnO nanoparticle doping. After heat treatment, it decreased down to 1.33 is due to the porosity. Faure et al. [35] reported that lower effective refractive index while avoiding excessive scattering is due to the nanosized porosity. Additionally, the refractive index of all samples is much lower than that of reported values of zinc oxide n = 2.02 [35], and titania n = 2.6, suggesting the porous structure of synthesized nanocomposites.

Thermal gravimetric analysis (TGA) and differential thermal analysis (DTA) is illustrated in Fig. 9(a–c) in the 30 °C - 1000 °C temperature range for SiO_2-TiO_2 nanocomposite, ZnO:SiO_2-TiO_2 nanocomposite and ZnO:SiO_2-TiO_2 nanocomposite after 1 h heating at 300 °C, respectively. Fig. 9(a) exhibited a TGA curve of SiO_2-TiO_2 nanocomposite which shows a maximum weight loss ~ 33.56% within the 60 °C–140 °C temperature range corresponding to the solvent and water volatilization of the gel films and condensation of SiO_2 and TiO_2 compounds, while, the minimum weight loss ~ 3.87% within the temperature range of 130 °C–345 °C suggests the thermal decomposition of organic components. After 400 °C, no significant changes were observed indicating that host SiO_2-TiO_2 nanocomposite is thermally stable. TGA curve of ZnO: SiO_2-TiO_2 sample [Fig. 9(b)] revealed the weight loss 11.08% and 28.95% in two temperatures ranges i.e. 30 °C–87 °C and 120 °C–995 °C. The first weight loss 11.08% is attributed to the loss of hydroxyl group, in continuation, the weight loss 28.95% is ascribed to the loss of acetate group and CTAB species, as documented in the literature [29], whereas, DTA curve exhibited three exothermic peaks at 65.33 °C, 164.45 °C and 228.25 °C [Fig. 9(b)] associated with the decomposition stages in TGA. The TGA and DTA analy-

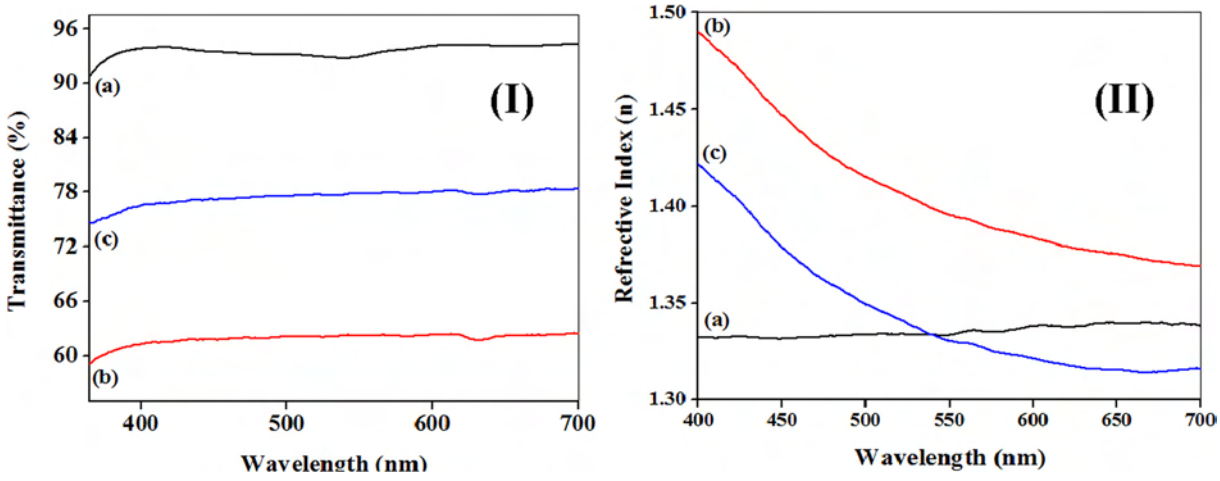

Fig. 8 (I) Transmission spectra of (a) SiO_2-TiO_2 nanocomposite (b) ZnO:SiO_2-TiO_2 nanocomposite (c) ZnO:SiO_2-TiO_2 nanocomposite after 1 h heating at 300 °C, (II) Dispersion of refractive index (a) SiO_2-TiO_2 nanocomposite (b) ZnO:SiO_2-TiO_2 nanocomposite (c) ZnO: SiO_2-TiO_2 nanocomposite after 1 h heating at 300 °C.

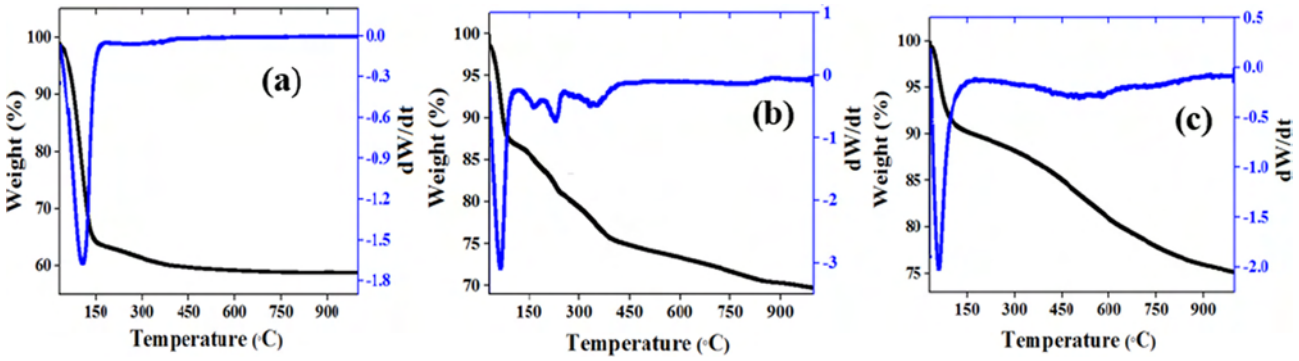

Fig. 9 Weight (%) versus temperature (°C) and [dW/dT] of (a) SiO_2-TiO_2 nanocomposite (b) ZnO:SiO_2-TiO_2 nanocomposite (c) ZnO: SiO_2-TiO_2 nanocomposite after 1 h heating at 300 °C.

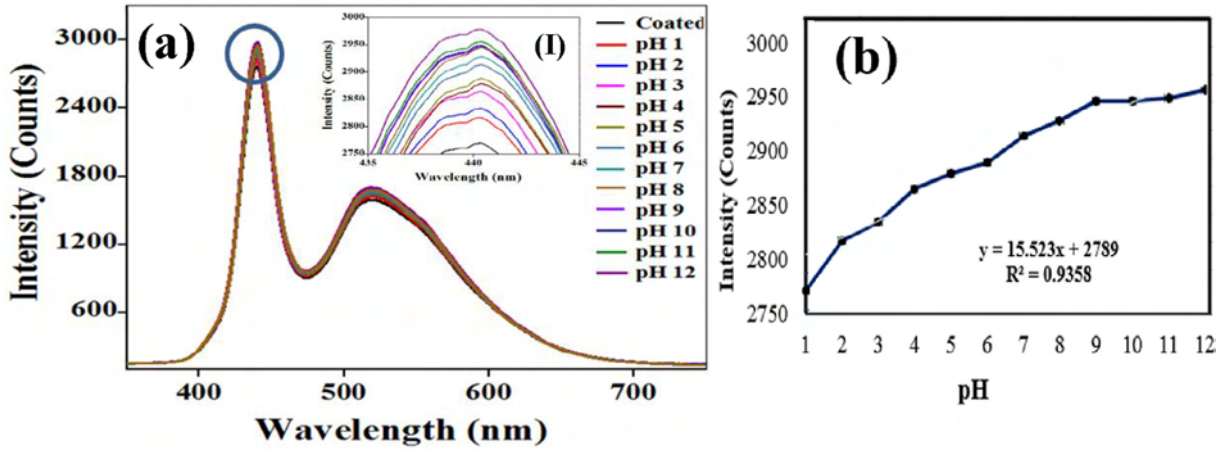

Fig. 10 (a). Optical spectra of mixed dyes encapsulated ZnO: SiO_2-TiO_2 nanocomposite coated on optical fiber treated with different pH ranges 1–12, inset (I) is the zoomed area of marked region, whereas, (b) is the sensitivity response of coated fiber within different pH values 1–12 at 440 nm.

ses of ZnO: SiO_2-TiO_2 sample after heat treatment [Fig. 9(c)] revealed that the weight loses ~ 7.84% at about 95 °C is accredited to the desorption/evaporation of solvents, and 16.32% weight loss at 100 °C–1000 °C suggesting a degradation of components into volatile combustible products. In the DTA curve an exothermic peak at 58 °C was probably due to the volatile organic moieties generated by the dissociation of precursors which is confirmed by the weight loss observed in the TGA curve.

The dye encapsulated ZnO: SiO_2-TiO_2 nanocomposite shows the transmission spectra of coated optic fiber in terms of output intensity variations within pH solutions 1–12 in Fig. 10(a). The spectra show a distinct, intense variation at the peak wavelength of 440 nm. The response of the coated fiber is found to be increased by increasing the pHs. Inset (I) is the zoomed area of marked region in Fig. 10(a). Fig. 10(b) shows the linear relationship between intensity and pH 1–12, suggesting the good interaction between coating species and light. The calculated sensitivity value is of 15 counts/pH with 93% repeatability at wavelength of 440 nm. Moreover, no leaching traces are inspected during measurement.

Fig. 11(a) shows the time response curve of dyes encapsulated ZnO: SiO_2-TiO_2 nanocomposite within different pH solutions 1–12. The prepared nanocomposite sol shows fast response ~0.50 s at pH 1 and ~0. 15 s at pH 12. Moreover, it can be seen visually that the dyes encapsulated ZnO: SiO_2-

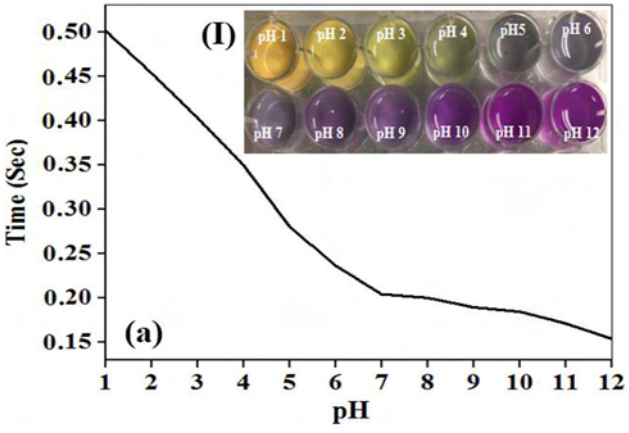

Fig. 11 (a) Time response of mixed dyes encapsulated ZnO: SiO_2-TiO_2 nanocomposite within different pH solutions 1–12, whereas, inset (I) is corresponding to the color variations.

TiO_2 nanocomposite exhibited orange color in acidic media which slightly changed into yellow, violet and finally purple by varying the pHs 1–12 as shown in inset of Fig. 11(a). The variations in color are due to H^+ and OH^- ions which freely penetrate into the mesoporous nanocomposite and reacting with dye species, results in color variations as documented in the literature [36]. The experimental findings suggest the strong interconnection between Zn: SiO_2-TiO_2 nanocomposite and dyes species which plays an effective role in stability of fiber optic sensing device.

5. Conclusion

Influence of ZnO doping on the sol-gel based SiO_2-TiO_2 nanocomposite is reported in this work for fiber optic pH sensing applications. Upon SiO_2-TiO_2 modifications, ZnO doping and heat treatment can control the stability and surface properties of modified nanocomposites matrix. Crack-free spherical morphology with good interaction of SiO_2 and TiO_2 species with zinc ions was observed by FESEM/EDX and AFM which is advantageous for sensing applications. TEM analysis shows that the prepared nanocomposites have spherical nanoparticles. XRD analysis confirmed the formation of new phase ZnSiO3 along with anatase phase of titania. Furthermore, heterogeneous bonded, high surface area, thermally stable nanocomposites has good transparency (92–62% in the visible range) with low refractive index 1.33–1.39 at the wavelength of 550 nm, which is confirmed by FTIR, BET and UV–Vis spectroscopy. The response of the ZnO:SiO_2-TiO_2 nanocomposite coated fiber optic sensor is optimized at pH 12 with fast response time 0.15 s. The observed sensitivity is of 15 counts/pH with repeatability of 93% at 440 nm. Thus, this study indeed suggested an effective modification of ZnO doped nanocomposite matrix for pH sensing at room temperature with visual color detection.

Acknowledgments

Dr. Shumaila Islam acknowledges the financial support provided by the Universiti Teknologi Malaysia, through RMC under the Postdoctoral Fellowship for the performance and management of the project. Corresponding author is grateful to the Malaysian Ministry of Education through the FRGS fund with vote 03E89.

References

[1] R.C. Pawar, D. Cho, C.S. Lee, Fabrication of nanocomposite photocatalysts from zinc oxide nanostructures and reduced graphene oxide, Curr. Appl Phys. 13 (2013) S50–S57.
[2] S. Islam, N. Bidin, S. Riaz, S. Naseem, Sol–gel based phenolphthalein encapsulated heterogeneous silica–titania optochemical pH nanosensor, J. Ind. Eng. Chem. 34 (2016) 258–268.
[3] R.N. Moussawi, D. Patra, Modification of nanostructured ZnO surfaces with curcumin: fluorescence-based sensing for arsenic and improving arsenic removal by ZnO, RSC Adv. 6 (2016) 17256.
[4] X.d. Wang, R.J. Meier, C. Schmittlein, S. Schreml, M. Schäferling, O.S. Wolfbeis, A water-spray able, thermogelating and biocompatible polymer host for use in fluorescent chemical sensing and imaging of oxygen, pH values and temperature, Sensors Actuators B: Chem. 221 (31) (2015) 37–44.
[5] C. Dey, T. Kundu, B.P. Biswal, A. Mallick, R. Banerjee, Crystalline metal-organic frameworks (MOFs): synthesis, structure and function, Acta Cryst. B 70 (2014) 3–10.
[6] A.K. Das, R.S. Vemuri, I. Kutnyakov, B.P. McGrail, R.K. Motkuri, An efficient synthesis strategy for metal-organic frameworks: dry-gel synthesis of MOF-74 framework with high yield and improved performance, Sci. Rep. (2016) 28050.
[7] Y. Wu, M. Yan, X. Liu, P. Lv, J. Cui, M. Meng, J. Dai, Y. Yana, C. Li, Accelerating the design of multi-component nanocomposite imprinted membranes by integrating a versatile metal–organic methodology with a mussel-inspired secondary reaction platform, Green Chem. 17 (2015) 3338.
[8] K.N. Abbas, N. Bidin, R.S. Sabry, H.J. Al-Asedy, M.A. Al-Azawia, S. Islam, Structures and emission features of high-density ZnO micro/nanostructure grown by an easy hydrothermal method, Mater. Chem. Phys. Xxx (2016) 1–10.
[9] S.A. Vanalakar, V.L. Patil, N.S. Harale, S.A. Vhanalakar, M.G. Gang, J.Y. Kim, P.S. Patil, J.H. Kim, Controlled growth of ZnO nanorod arrays via wet chemical route for NO2 gas sensor applications, Sensors Actuators B 221 (2015) 1195–1201.
[10] M.K.S. Li, P. Gao, P. Yue, X. Hu, Synthesis of exfoliated CNT–metal–clay nanocomposite by chemical vapor deposition, Sep. Purif. Technol. 67 (2) (2009) 238–243.
[11] R. Iordanova, R. Gegova, A.B. Nedelcheva, Y. Dimitriev, Sol-gel synthesis of composites in the ternary TiO_2–TeO_2–B_2O_3 system, Eur. J. Glass Sci. Technol. B Phys. Chem. Glasses 56 (4) (2015) 128–138.
[12] J. Bahadur, D. Sen, S. Mazumder, P.U. Sastry, B. Paul, H. Bhatt, S.G. Singh, One-step fabrication of thermally stable TiO2/SiO2 nanocomposite microspheres by evaporation-induced self-assembly, Langmuir 28 (31) (2012) 11343–11353.
[13] S. Islam, N. Bidin, S. Riaz, G. Krishnan, S. Naseem, Sol–gel based fiber optic pH nanosensor: structural and sensing properties, Sensors Actuators A. 238 (2016) 8–18.
[14] M.A. Ghanem, N.H. Khdary, A.M. Almayouf, M.A. Salah, Synthesis and characterizations of titanium tungstophosphate nanoparticles for heavy metal ions removal, Solid State Phenom. 257 (2017) 187–192.
[15] A.M. Ali, A.A. Ismail, H. Bouzid, F.A. Harraz, Sol–gel synthesis of ZnO–SiO2 thin films: impact of ZnO contents on its photonic efficiency, J. Sol-Gel Sci. Technol. 71 (2) (2014) 224–233.
[16] N.H. Using, B. Launay, G. Kickelbick, Silica-Titania mesostructured films, J. Sol-Gel Sci. Technol. 26 (2003) 615–619.
[17] P. Biswas, F. Chiavaioli, S. Jana, N. Basumallick, C. Trono, A. Giannetti, S. Tombelli, A. Mallick, F. Baldini, S. Bandyopadhyay, Design, fabrication and characterization of silica-titania thin film coated over coupled long period fibre gratings: towards bio-sensing applications, Sens. Actuators, B 253 (2017) 418–427.
[18] F. Aslan, A. Tumbul, A. Goktas, R. Budakoglu, B.H. Mutlu, Growth of ZnO nanorod arrays by one-step sol–gel process, J. Sol-Gel Sci. Technol. 80 (2016) 389–395.
[19] Z. Nenova, T. Nenov, S. Kozhukharov, M. Machkova, Humidity sensing elements based on Zn-doped TiO2 films prepared via a sol-gel method, Mater. Sci. 21 (2) (2015) 191–197.
[20] Z. Qinqin, J. Dianxing, D. Xiaolong, H.C. Jinzhao, X. Bingqiang, Morphology-modulation of SnO2 hierarchical architectures by Zn doping for glycol gas sensing and photocatalytic applications, Sci. Rep. 5 (2015) 7874.
[21] S. Islam, N. Bidin, S. Riaz, S. Naseem, J. Sol-Gel Sci. Technol. (2017), https://doi.org/10.1007/s10971-017-4523-8.
[22] R. Singh, B.C. Yadav, Synthesis and characterization of copper doped tin oxide for humidity sensing applications, Adv. Sci. Lett. 20 (2014) 895–902.

[23] O.B. Miled, H.B. Ouada, J. Livage, pH sensor based on a detection sol–gel layer onto optical fiber, Mater. Sci. Eng., C 21 (1–2) (2002) 183–188.
[24] M. Kim, E. Park, H. Jung, S.-T. Yun, J. Jurng, Temperature-dependent thermal stability and dispersibility of SiO_2–TiO_2 nanocomposites via a chemical vapor condensation method, Powder Technol. 267 (2014) 153–160.
[25] A.G. Howard, N.H. Khdary, Spray synthesis of monodisperse sub-micron spherical silica particles, Mater. Lett. 61 (8–9) (2007) 1951–1954.
[26] M. Thirumavalavan, K.L. Huang, J.F. Lee, Preparation and morphology studies of nano zinc oxide obtained using native and modified chitosans, Materials 6 (2013) 4198–4212.
[27] S. Singh, A. Singh, M. Wana, R.R. Yadav, P. Tandon, S.S.A. Rasool, B.C. Yadav, Fabrication of self-assembled hierarchical flowerlike zinc stannate thin film and its application as liquefied petroleum gas sensor, Sens. Actuators B: Chem. 205 (2014) 102–111.
[28] S. Riaz, R. Ashraf, A. Akbar, S. Naseem, Free growth of iron oxide nanostructures by sol–gel spin coating technique-structural and magnetic properties, IEEE Trans. Magn. 50 (8) (2014) 2301805.
[29] M.F. Khan, A.H. Ansari, M. Hameedullah, E. Ahmad, F.M. Husain, Q. Zia, U. Baig, M.R. Zaheer, M.M. Alam, A.M. Khan, Z.A. Al-Othman, I. Ahmad, G.M. Ashraf, G. Aliev, Sol-gel synthesis of thorn-like ZnO nanoparticles endorsing mechanical stirring effect and their antimicrobial activities: potential role as nano-antibiotics, Sci. Rep. 6 (2016) 1–12.
[30] A. Mourhly, M. Khachani, A. El Hamidi, M. Kacimi, M. Halim, S. Arsalane, The synthesis and characterization of low-cost mesoporous silica SiO_2 from Local Pumice Rock, Nanotechnol. Nanomater. 5 (35) (2015) 1–7.
[31] S. Rasalingam, R. Peng, R.T. Koodali, Removal of hazardous pollutants from wastewaters: applications of TiO_2-SiO_2 mixed oxide materials, J. Nanomater. 2014 (2014), 42 pages 617405.
[32] S. Islam, N. Bidin, S. Riaz, L.P. Suan, S. Naseem, M.M. Sanagi, Mesoporous nanocomposite coatings for photonic devices: sol–gel approach, Appl. Phys. A 122 (2016) 935.
[33] R.D.P. Andrade, R.M. Lemus, C.E.C. Perez, Models of sorption isotherms for food: uses and limitations, Vitae, Revista De La Facultad De Quomica Farmaceutica 18 (3) (2011) 325–334.
[34] S. Chhatre, V. Aravindan, D. Puthusseri, A. Banerjee, S. Madhavi, P.P. Wadgaonkar, S. Ogale, High surface area porous carbon for ultra-capacitor application by pyrolysis of polystyrene containing pendant carboxylic acid groups prepared via click chemistry, Mater. Today Commun. 4 (2015) 166–175.
[35] B. Faure, G.S. Alvarez, A. Ahniyaz, I. Villaluenga, G. Berriozabal, Y.R.D. Miguel, L. Bergstrom, Dispersion and surface functionalization of oxide nanoparticles for transparent photocatalytic and UV-protecting coatings and sunscreens, Sci. Technol. Adv. Mater. 14 (2013) 23pp.
[36] F. Maia, J. Tedim, A. Bastos, M.G.S. Ferreira, M.L. Zheludkevich, Nanocontainer-based corrosion sensing coating, Nanotechnology 24 (2013) 415502.